Extrinsic interface formation of HfO_2 and Al_2O_3/GeO_x gate stacks on Ge (100) substrates

H. Seo,[1] F. Bellenger,[2] K. B. Chung,[3] M. Houssa,[4] M. Meuris,[2] M. Heyns,[2] and G. Lucovsky[3,a)]

[1]*Materials Sciences Division, Lawrence Berkeley National Laboratory, Berkeley, California 94720, USA and University of California, Berkeley, California 94720, USA*
[2]*IMEC, Kapeldreef 75, B-3001 Leuven, Belgium*
[3]*Department of Physics, North Carolina State University, Raleigh, North Carolina 27695, USA*
[4]*Department of Physics and Astronomy, University of Leuven, B-3001 Leuven, Belgium*

(Received 12 March 2009; accepted 13 July 2009; published online 26 August 2009)

The extrinsic interfaces present at the $HfO_2/GeO_x/Ge$ and $Al_2O_3/GeO_x/Ge$ gate stacks are investigated. The effective trapped charge density, estimated from hysteresis in capacitance-voltage characteristics, is higher for HfO_2 than for Al_2O_3, implying qualitatively different charge trapping sources in each dielectric. Spectroscopic ellipsometry and medium energy ion scattering measurements reveal that HfO_2 deposition induces the formation of a thicker germanate (intermixed) layer at the HfO_2/GeO_x interface, where nonstoichiometric Ge-rich GeO_x having significantly low bandgap (~ 1.8 eV) is present. In contrast, Al_2O_3 deposition leads to an abrupt and thinner O-rich GeO_x interfacial layer without Ge-rich GeO_x phase. The proposed band alignment indicates that Ge-rich GeO_x layer at HfO_2/GeO_x arises a significant band potential well trapping, while O-rich GeO_x layer in Al_2O_3/GeO_x is responsible for a relatively lower charge trapping at band potential well. The combined results strongly suggest that the control of the GeO_x interface layers is crucial to reduce the high charge trapping at high-$\kappa/GeO_x/Ge$ gate stacks. © *2009 American Institute of Physics*. [DOI: 10.1063/1.3204026]

I. INTRODUCTION

There have been considerable research efforts in order to achieve Ge-based metal-oxide-semiconductor field effect transistor (MOSFET) since Ge channel provides higher and symmetric intrinsic mobility for both electrons and holes as compared to Si. Previous studies revealed that Ge-based MOSFETs exhibit a hole mobility that is two times higher than that in Si, leading to a corresponding increase in the *p*-FET drain current.[1] Nevertheless, Ge-based MOSFETs usually suffer from inferior interfacial properties between the Ge channel, the interfacial oxide, and the high-κ gate dielectrics.[2,3] This interfacial problem is mainly responsible to the large capacitance-voltage (*C-V*) hysteresis and extremely low *n*-FET mobility.

In this regard, several approaches to achieve high-quality Ge interfaces have been investigated using various interfacial passivation, such as GeO_x, GeO_xN_y, and Si.[3–6] Although the physical reason for the degraded interfacial quality is still vague, a recent study reports that the fast interface state density of high-κ/GeO_x-passivated Ge gate stack is in fairly good level on the order of 10^{11} cm^{-2} eV^{-1}.[7] This fact strongly imposes the need of in-depth studies focusing on the more pronounced degradation of interfaces between GeO_x passivation interlayer and high-κ gate dielectrics.

In this study, we have characterized the interfacial region between two different high-κ gate dielectrics (HfO_2 and Al_2O_3) and thermally grown GeO_x interlayers. A defect state present near the conduction band (CB) edge has been identified by visible-ultraviolet (VUV) spectroscopic ellipsometry (SE) measurements guided by a concise optical stack modeling of the absorption data. The spatial distribution of species at the interface has been evaluated by medium energy ion scattering (MEIS). These results have been correlated with the electrically determined oxide trapped charges in the gate stack.

II. EXPERIMENTAL

The *n*- and *p*-type Ge (100) wafers were chemically treated with $NH_4OH/H_2O_2/H_2O$, followed by a 2% HF dip, resulting in a clean Ge surface. The prepared Ge samples were loaded into an ASM Polygon 8200 cluster tool equipped with an Epsilon reactor for thermal treatments and an atomic layer deposition (ALD) Pulsar 2000 reactor for high-κ deposition. Before introducing O_2 gas in the reactor, the samples were annealed in H_2 at 650 °C for 10 min to desorb the native GeO_x layer. Oxidation was then carried out at a low temperature (between 350 and 450 °C) and a high partial pressure (1 atm) of O_2 having thickness of either about 1 or 2 nm. 2, 4, and 8 nm thick HfO_2 and Al_2O_3 layers were then deposited at 300 °C by ALD using $HfCl_4$ or trimethylaluminum precursors with H_2O as the oxidant. The H_2 anneal, the Ge oxidation, and the high-κ deposition were all done *in situ*. The $HfO_2/GeO_x/Ge$ and $Al_2O_3/GeO_x/Ge$ gate stacks were characterized by VUV SE working in rotating compensator configuration and MEIS.

To fabricate MOS capacitors, the TiN layer was deposited on the gate stack by sputtering, followed by photolithography, and a final N_2 anneal at 550 °C for 5 min. The elec-

a)Electronic addresses: lucovsky@ncsu.edu

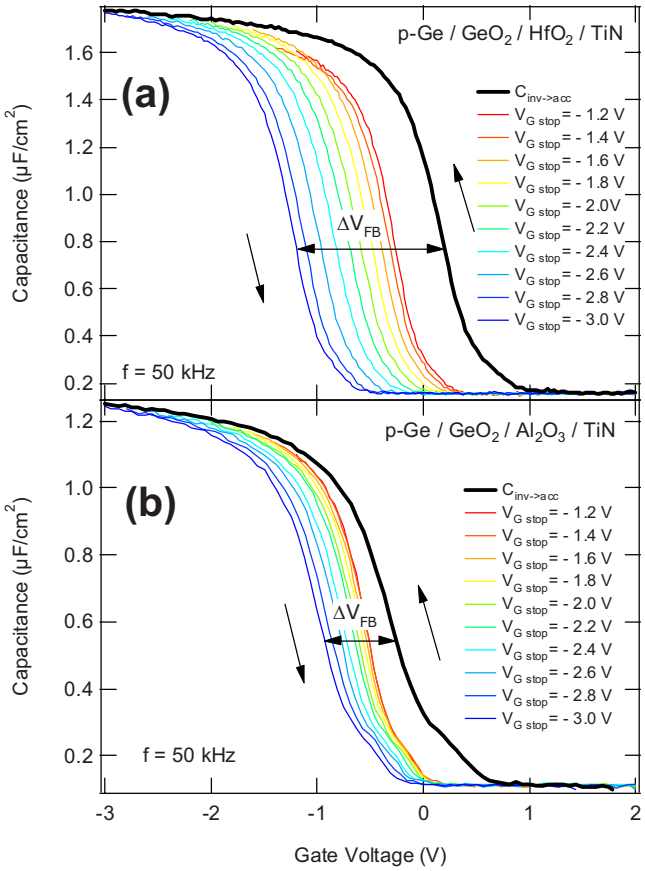

FIG. 1. (Color online) *C-V* hysteresis traces for different turnaround gate voltages ($V_{G\ \mathrm{stop}}$) varied between −1.2 V (rightmost downward red curve) and −3 V (leftmost downward blue curve) for (a) TiN/HfO_2 and (b) TiN/Al_2O_3 on GeO_x/*p*-Ge capacitors. In one *C-V* hysteresis measurement cycle, gate voltage was ramped up from inversion region ($V_{G\ \mathrm{start}}$: +2 V) to accumulation region ($V_{G\ \mathrm{stop}}$) for $C_{\mathrm{inv}\rightarrow\mathrm{acc}}$ measurements (black curve) and then ramped down reversely from $V_{G\ \mathrm{stop}}$ to $V_{G\ \mathrm{start}}$ for ΔV_{fb} measurements. This cycle was repeated for different $V_{G\ \mathrm{stop}}$. The ramping up curve for $C_{\mathrm{inv}\rightarrow\mathrm{acc}}$ is constant regardless of $V_{G\ \mathrm{stop}}$ so that only one ramping up curve up to −3 V of $V_{G\ \mathrm{stop}}$ is plotted.

trical properties of MOS capacitors were characterized by capacitance-voltage (*C-V*) and current-voltage (*I-V*) measurements.

III. RESULTS AND DISCUSSION

Figures 1 and 2 present the *C-V* hysteresis and trapping efficiency of HfO_2 and Al_2O_3/GeO_x gate stacks evaluated by the correlation between the effectively trapped charge density (N_{eff}), determined by the flat band voltage shift (ΔV_{fb}) in *C-V* hysteresis measurements, and the injected charge density (N_{inj}), estimated from the current injected during the *C-V* sweeps, as expressed by following equations:

$$N_{\mathrm{eff}} = \frac{C_{\mathrm{fb}} \Delta V_{\mathrm{fb}}}{q}, \tag{1}$$

$$N_{\mathrm{inj}} = \frac{J_{G(V_{G_{\mathrm{stop}}})} \Delta t}{q}, \tag{2}$$

where C_{fb} is the capacitance at the flat band voltage, ΔV_{fb} is the difference in the flat band voltages in the hysteresis *C-V* curve, $J_{G(V_{G_{\mathrm{stop}}})}$ [from leakage current density-voltage (*J-V*) curves in Fig. 3] is the leakage current density at the stop voltage of ramping up curve, and Δt is the average time that the constant dc voltage (at $V_{G_{\mathrm{stop}}}$) is on hold for *C-V* measurement. In other words, N_{inj} corresponds to an upper average limit for the injected charge density.

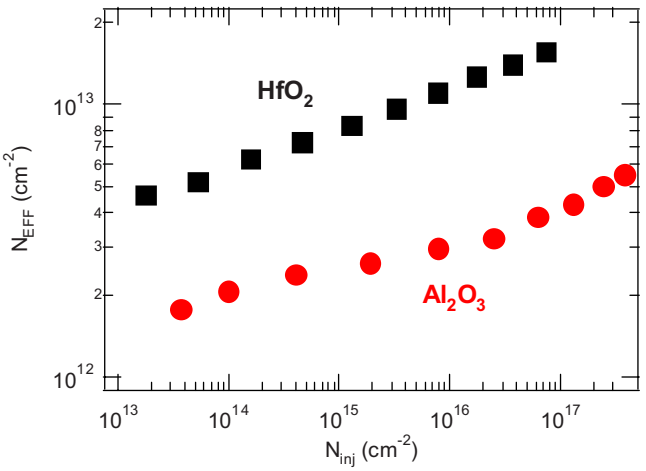

FIG. 2. (Color online) Effectively trapped charge density (N_{eff}) determined by the flat band voltage shifts (ΔV_{fb}) in *C-V* hysteresis measurements vs injected charge density (N_{inj}) determined from the current injected during the *C-V* sweep.

It is noted that the hysteresis *C-V* traces of both of HfO_2 and Al_2O_3 gate stacks revealed the negative ΔV_{fb}, which is equivalent to the positive charge trapping. The hysteresis *C-V* traces measured at 50 kHz goes into the depletion mode under positive gate bias so that there is a very limited amount of minority charge carriers (i.e., electron) available for substrate injection and subsequent trapping at the gate oxide stacks. This poses the higher majority carrier (i.e., hole) injection from *p*-type Ge substrate and trapping under the negative gate bias rather than electron trapping under the positive gate bias during hysteresis *C-V* measurements. Chung *et al.* reported the counterpart *C-V* hysteresis results on *n*-Ge/GeON/HfO_2 MOS capacitors annealed at different temperatures.[8] In this report, hysteresis *C-V* traces revealed

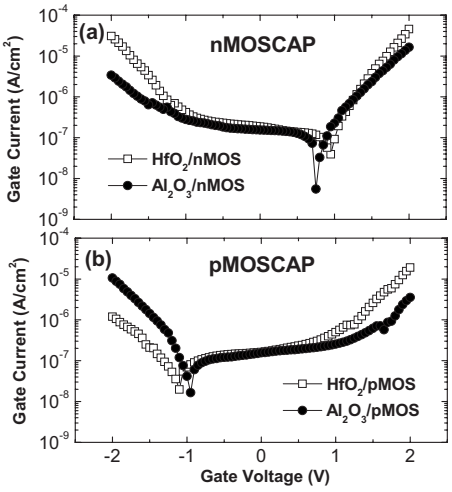

FIG. 3. Gate leakage current-voltage plots for (a) HfO_2 and Al_2O_3 of *n*-Ge MOS capacitor and (b) HfO_2 and Al_2O_3 of *p*-Ge MOS capacitor. The current level at the given gate voltage in this plots was used for the estimation of injected charge density (N_{inj}) in Eq. (2).

the positive ΔV_{fb}, which is equivalent to the negative charge (electron) trapping at N_{eff} of mid-10^{12} cm^{-2}, i.e., a majority charge trapping under positive bias in the accumulation mode. Therefore, it is suggested that the amphoteric trapping source is present at the interface between Ge oxides and HfO_2. This will be discussed in detail with the proposed band diagram model in Fig. 6.

At the same N_{inj}, the HfO_2 gate stack shows a larger ΔV_{fb}, i.e., a larger density of trapped charges at gate oxide stacks, as compared to Al_2O_3. For example, 10^{17} cm^{-2} for N_{inj} results in 10^{13} cm^{-2} for N_{eff} for HfO_2, which is almost an order of magnitude larger trapped charge density than Al_2O_3. This N_{eff} level in the HfO_2/GeO_x gate stacks is surprisingly larger compared to many reports about HfO_2 on Si substrate.[9]

Figure 3 represents *J-V* curves in both *n*-Ge and *p*-Ge MOS capacitors. As aforementioned, *J* levels are much higher under the gate bias condition corresponding to the accumulation mode for each Ge substrate (i.e., positive bias for *n*-Ge and negative bias for *p*-Ge MOS capacitor). In addition, asymmetric V_{fb} shift in *J-V* curves between *n*-Ge and *p*-Ge capacitors are observed: the positive V_{fb} shift for *n*-Ge and the negative V_{fb} shift for *p*-Ge MOS capacitors. Therefore, differences in *J-V* results between *n*-Ge and *p*-Ge MOS capacitors reinforce the majority charge trapping at the interfaces.

It is well known that nanocrystalline HfO_2 is subject to the localized oxygen vacancy defects when annealed at high temperature (>900 °C). This has been characterized as a main charge trapping source by forming discrete and shallow trap levels in the forbidden gap.[10] However, HfO_2/GeO_x gate stacks in the current study have been processed at low temperatures (<600 °C) and, furthermore, the measured trapped charge density is much larger than typical pre-existing defect levels in nanocrystalline HfO_2. Therefore, another possible trapping source other than localized oxygen vacancy defects is suspected to explain the unusual large *C-V* hysteresis. The clarification of the physical origins of trapping in these gate stacks has been studied using SE and MEIS.

Absorption coefficient spectra for gate stacks with different thicknesses of GeO_x and high-κ dielectrics are shown in Fig. 4. These spectra have been obtained from four-phase model extraction for the pseudodielectric function.[11] The simple model for a general four-phase model in SE analysis accounts for discrete homogeneous medium of the underlying substrate by stacking pure GeO_2 on Ge as a substrate model and then extraction of overlayer (HfO_2) with respect to the modeled GeO_2/Ge interface. However, this model is not suitable for this kind of gate stack since it appeared as having nonstoichiometric and nonlocal GeO_x rather than GeO_2. Following a previous analysis on suboxide layers of SiO_2 on Si,[11] four-phase modeling was also employed on these gate stacks. The best reference in this model was the suppression of artifacts in dielectric function below a bandgap of high-κ dielectrics, which are the strained Ge CB states peak at approximately 2.3 and 4.2 eV. As a result, the best interlayer GeO_x model for HfO_2 stack was achieved by considering 0.7 and 2 nm thick layers having a mixed phase of

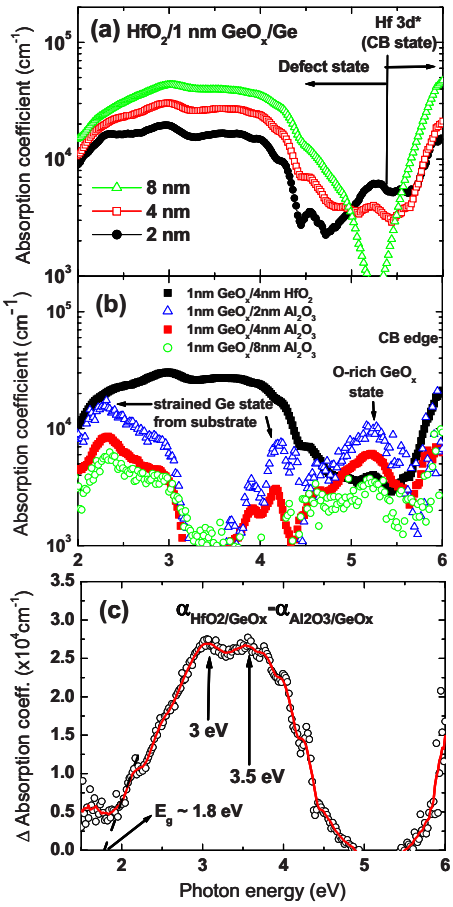

FIG. 4. (Color online) Absorption coefficient spectra from SE measurement of (a) HfO_2 with different thicknesses (2/4/8 nm) on 1 nm GeO_x interlayer and (b) 4 nm HfO_2 and 2/4/8 nm Al_2O_3 on 1 nm GeO_x. (c) Differentiated absorption spectra of 4 nm HfO_2 with respect to 4 nm Al_2O_3 on 1 nm GeO_x as in (b).

amorphous-$Ge_{0.5}$ and $(GeO_2)_{0.5}$ constructed by effective medium approximation[12] in a circular medium shape of each phase, corresponding to 1 and 2 nm declared GeO_x thickness based on transmission electron microscopy images, respectively. This is a very crucial step in SE analysis for discriminating the real overlayer states from the artifact features of strained Ge having several tens of meV shift from states on a clean Ge surface.

In Fig. 4(a), the states above 5.5 eV are associated with the intrinsic CB state of empty Hf $5de_g^*$ (antibonding) state. All the HfO_2 layers show the absorption onset from 5.5 eV. In addition to the intrinsic CB states of HfO_2, two different subband edge states are observed. The first peak state at 5.2 eV observed in both Al_2O_3 and HfO_2 [Fig. 4(b)] is assigned as the CB edge state of the GeO_x interlayer. This GeO_x layer shows the lower bandgap at 4.6 eV determined by extrapolation of 5.2 eV peak state than bulk stoichiometric GeO_2 because it is nonstoichiometric GeO_x ($x<2$) or, equivalently, O-rich GeO_x.[13] The second broad states observed between 2 and 5 eV are unusual for typical HfO_2 layers on Si even if considering the discrete Hf^{3+} or oxygen vacancy states present in the forbidden gap of nanocrystalline HfO_2. These gap states of HfO_2/GeO_x are broader and more extended over the whole energy gap range. In particular, the absorption of these gap states is more pronounced in

thicker HfO_2 layers. This observation implies that these gap states strongly depend on the HfO_2 deposition on the GeO_x interlayers. It was proposed that some chemical reaction during HfO_2 deposition, e.g., the formation of hydroxyl groups, could turn GeO_x to be chemically unstable.[14] Therefore, we suspect that the HfO_2 deposition on the GeO_x interlayer induces intermixing between the two layers, leading to the formation of a germanate layer and thus to gap states in the absorption spectra of HfO_2.

The specific origin of these gap states can be considered by two possible sources as expected in the discussion on *C-V* analysis. The first possible origin is the bonding defects existing in the local border of HfO_2 in the vicinity of the interfaces and/or in the interfacial germanate layer itself. This bonding defect physically originates from the bond coordination mismatch of sevenfold nanocrystalline HfO_2 and three- or fourfold GeO_x based on bond constraint theory.[15] This bonding defect at the border was assigned as a major defect source in chemically phase separated Hf silicate.[15] However, localized defect associated states in the absorption spectra are much shallower to CB edge and have discrete bandwidth (0.5–1 eV) in contrast to the spectra in Fig. 4(a). The spectroscopic feature of the localized defect states in nanocrystalline HfO_2 is due to the intrinsic property of transition between oxygen vacancy induced occupied and empty Hf^{3+} molecular orbital states. Since it is apparent that spectral features observed for the gap state in this work are different from the spectral features of typical Hf^{3+} states associated with defects in nanocrystalline HfO_2, another possible origin of gap states for HfO_2/GeO_x should be considered in this study.

As a more possible origin, the lower bandgap of nonstoichiometric GeO_x layer is considered. There are several reports on low bandgap nonstoichiometric GeO_x on Ge surfaces, which is observed in the transition from Ge to stoichiometric GeO_2.[16,17] In analogous to those reports, we suspect that chemical mixing between HfO_2 and GeO_x resulted in nonstoichiometric phase of Ge-rich GeO_x, where Ge–Ge bond second neighbors are involved in primary Ge–O–Ge bonds.

The current argument concerning the presence of Ge-rich GeO_x is experimentally supported by the absorption spectra and x-ray photoelectron spectroscopy (XPS) results. Figure 4(c) represents the differentiated absorption spectra of HfO_2 with respect to Al_2O_3. In the absorption spectra, the bandgap of HfO_2 at 5.5 eV is assigned by the extrapolation of strong absorption onset edge. Because of the limited range of incident photon energy for SE analysis, it is not possible to determine the bandgap of Al_2O_3 directly from the spectra in Fig. 4(b), but it should be larger than 6 eV since strong absorption onset in Fig. 4(b) is not observed as well as the bandgap of the same 4 nm Al_2O_3 was declared as 6.1 eV in the other report.[2] Since these dielectrics are optically transparent up to their direct bandgaps, the resultant spectrum in Fig. 4(c) reflects the clear difference in absorption at the GeO_x interfacial layers between HfO_2 and Al_2O_3 gate stacks. The differentiated spectrum in Fig. 4(c) presents the absorption onset at about 1.8 eV and tentatively assigned peak states at 3 and 3.5 eV, although the peak intensities are relatively weak because the absorption in the GeO_x interface at ~1 nm is very weak. The intensity of the reflected beam from the GeO_x interface is attenuated in the upper high-κ dielectric layer during the beam propagation to the surface. However, it is noted that these spectral features are similar to the reported GeO_x spectra.[16] As in Ref. 16, Ge-rich GeO_x suboxide species was formed in the transition from Ge to fully oxidized GeO_2 and this GeO_x was reported to reveal a significantly lower bandgap at 1.5 eV and correlated peaks at 3.1 and 3.5 eV. Although interfacial chemistry in this study is related to intermixing of GeO_2 and HfO_2, the similarity of the spectra to a previous report on GeO_x on Ge implies that the presence of Ge-rich GeO_x is highly possible.

As additional supporting evidence for this argument, XPS analysis[7] on the HfO_2/GeO_x stack showed the much lower Ge^{4+} fraction out of all 1–4+ Ge oxidation states at 10% compared to that of the Al_2O_3/GeO_x stack at 90%. Therefore, the combined results of the absorption spectrum in Fig. 4(c) and XPS result in Ref. 7 suggest that Ge–Ge bonds formed by the chemical instability in GeO_2 replace Ge–O bonds and, as a result, led to a great amount of loss of full oxidation state, Ge^{4+}, in HfO_2/GeO_x. There is a similar report on nonstoichiometric GeO_x formation at the HfO_2/Ge interfaces.[12] In this report, HfO_2 is grown by e-beam evaporation without any heating so that this instability of the HfO_2/GeO_x interface might be chemically intrinsic and is independent of the deposition method.

In contrast to HfO_2, the absorption spectra of Al_2O_3 shown in Fig. 4(b), do not reveal any noticeable gap states, as in HfO_2. Furthermore, Al_2O_3 shows the decrease in the intensity of gap states as a function of thickness, which is a reverse trend to HfO_2; (i) the systematic decrease in strained Ge state features at 2.3 and 4.3 eV, backreflected from Ge surface, and (ii) weaker 5.2 eV peak related to O-rich GeO_x state as going to thicker Al_2O_3 layers. These trends in the absorption spectra of Al_2O_3 imply that the physical locations of interfacial reflection responsible for gap states are different from HfO_2. The interfacial Ge-rich GeO_x in the GeO_x/HfO_2 stack extends toward the surface through the HfO_2 layer with thicker HfO_2 deposition and therefore it produces the stronger absorption of gap states from Ge-rich GeO_x with thicker HfO_2. On the other hand, the interfacial O-rich GeO_x does not extend depending on Al_2O_3 deposition but tends to be more separated from the Al_2O_3 top surfaces, which lead to the higher intensity attenuation of the reflected light at strained Ge states and O-rich GeO_x states in the interfaces during the light propagation through thicker (e.g., 8 nm) Al_2O_3 than thinner (e.g., 2 nm) Al_2O_3. Similar to HfO_2, ALD process of Al_2O_3 also possibly leaves residual hydroxyl groups on the GeO_x surfaces, potentially causing chemical instability of GeO_x. However, it is a common knowledge that Al_2O_3 does not react with the oxide interlayer (e.g., SiO_2), resulting in more abrupt interfaces than HfO_2. In other words, germanate formation is greatly suppressed in the case of Al_2O_3 deposition, as compared to HfO_2, confirmed in Fig. 4(b). Indeed, the best interfacial model in four-phase modeling of Al_2O_3 stacks for SE analysis corresponds to GeO_2-rich mixed phase of

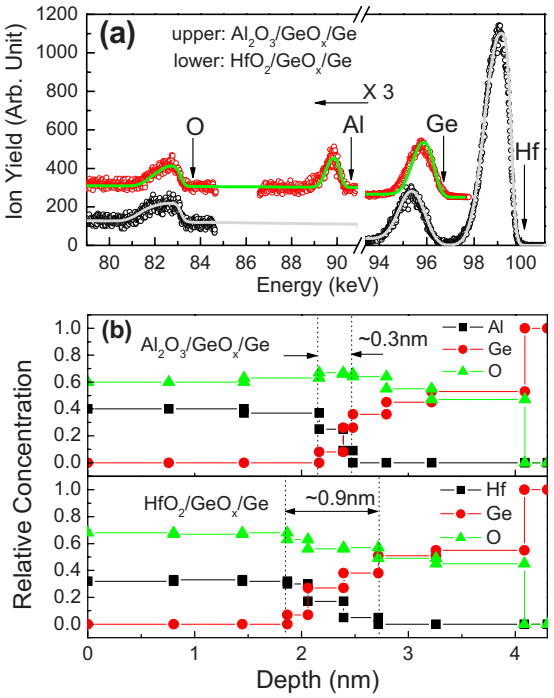

FIG. 5. (Color online) (a) MEIS energy spectra for 2 nm HfO_2 and Al_2O_3 on 1 nm GeO_x and (b) depth profiles constructed from a simulation of the spectra in (a).

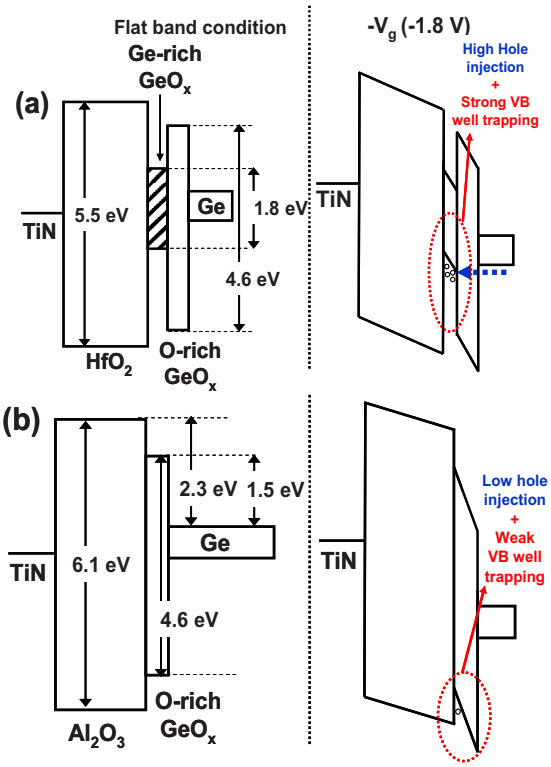

FIG. 6. (Color online) Schematic band alignment of gate stacks in *p*-Ge MOS capacitors for (a) HfO_2/Ge-rich GeO_x/O-rich GeO_x and (b) Al_2O_3/O-rich GeO_x interfaces.

amorphous-$Ge_{0.2}$ and $(GeO_2)_{0.8}$. Again, this is consistent with Ge^{4+} rich oxidation state observed from XPS results on the Al_2O_3/GeO_x stacks in Ref. 7.

From comparison of SE absorption and XPS data on HfO_2 and Al_2O_3/GeO_x, it is certain that the chemical instability of GeO_x is greatly affected by high-κ dielectrics.

In order to investigate the change in concentration in the depth direction, MEIS analysis was performed with a 100 keV proton ion beam in the double alignment condition, which eliminates contributions from crystalline Ge substrates. The incident beams were aligned in the [111] direction, and the scattered beams were aligned along the [001] direction with a scattering angle of 125°. In the energy spectra of Fig. 5(a), the peak width of Ge and O (higher and lower energy edges, respectively) are broader in the HfO_2 stack, as compared to the Al_2O_3 stack. This extended energy distribution of Ge and O species in HfO_2 is likely due to the thicker interfacial germanate layer formed as a result of HfO_2 deposition on the GeO_x interlayer. The depth profile obtained by the elemental density adapted simulation[16] on the energy spectra unambiguously reveals that HfO_2 has the thicker interfacial germanate layer ($\sim$0.9 nm), as compared to the mixed layer in Al_2O_3 ($\sim$0.3 nm). More importantly, the Ge relative concentration is higher in the hafnium germanate layer. As a result, the layer thickness, over which the composition changes, is distinctly different between HfO_2 and Al_2O_3 gate stacks. We regard that this 0.9 nm interfacial layer at HfO_2/GeO_x identified in MEIS spectra is related to Ge-rich GeO_x layer since it has explicitly different properties from Al_2O_3: (i) physically thicker layer and (ii) more Ge contents of interfaces.[18]

Conversely, Al_2O_3 depth profile shows an abrupt interface with uniform relative concentration of all species. Therefore, analysis on MEIS spectra reinforces that the interfacial characteristics are strongly related to high-κ overlayer on GeO_x.

Based on all of the discussed electrical and spectroscopic data supposing Ge-rich GeO_x presence at HfO_2/GeO_x and O-rich GeO_x at Al_2O_3/GeO_x, the band alignment across gate stack under flat band and negative gate bias (−1.8 V) condition is proposed in Fig. 6. The Ge-rich GeO_x interfacial layer having 1.8 eV of bandgap, inferred from Fig. 4(c), is assumed to be present at the HfO_2/GeO_x interface. In fact, there is an uncertainty in the proposed band alignment on the band offset of Ge-rich GeO_x with respect to Ge. These should be studied further by other experimental approaches, but reasonable estimation based on other reports[14,19] yields a CB offset of 0.5 ± 0.1 eV and valence band (VB) offset of 0.7 ± 0.1 eV for Ge-rich GeO_x with respect to Ge. The bandgap of the thermally grown O-rich GeO_x was assigned as 4.6 eV from SE measurement. Other band offsets between Ge and high-κ/GeO_x dielectrics have been determined by a previous study.[14]

It is obvious from the band alignment that the interfacial Ge-rich GeO_x acts as CB and VB potential wells as trapping sources for both electrons and holes. Under a negative applied bias condition for *p*-Ge, the charge (hole) trapping in the gate stack is modeled as shown in Fig. 6. First, holes tunnel through thermally grown GeO_x (O-rich GeO_x) by Fowler–Nordheim first and are trapped in VB potential well of Ge-rich GeO_x between HfO_2 and O-rich GeO_x. While trapping efficiency at localized oxygen vacancy defects in high-κ dielectrics and interfaces are typically limited by pre-existing defect density ($\sim$mid-10^{18} cm^{-3} or low-10^{12} cm^{-2}

for nanocrystalline HfO_2), the empty states for trapping in Fig. 6(a) are VB well, and therefore, the effective density of state in VB of GeO_x is a limiting factor which is supposed to be large enough to accommodate more injected charges at $\sim 10^{13}$ cm^{-2} from the Ge substrate. In this charge trapping scheme, several important points with consideration on low bandgap Ge-rich GeO_x should be noted. Both electrons and holes can be trapped at this Ge-rich GeO_x interface because it has the potential well both in CB and VB. In the *p*-type Ge capacitors used in this study, only the hole as a majority carrier is available for trapping under the negative V_G but in the real *n*-FET operation, electron as a minority carrier in an inversion layer of the channel can be trapped under the positive V_G as well. For *p*-FET operation, similar trapping occurs, but charges are vice versa. Secondly, one can assume that electrons are injected from gate electrode. However, as shown in Fig. 6, the probability of electron trapping under the gate injection is relatively lower than hole trapping under substrate injection since the physical thickness of HfO_2 (~ 4 nm) for electron tunneling is larger than the O-rich GeO_x layer (~ 1 nm).

Al_2O_3/GeO_x has no interfacial Ge-rich GeO_x as inferred from SE and MEIS measurements, and thus significant charge trapping as observed in HfO_2/GeO_x does not occur. However, trapped charge density of Al_2O_3/GeO_x in Fig. 2 is still higher level at low-10^{12} cm^{-2} than reported oxide trapped density of the Al_2O_3/SiO_2 stack at mid-10^{11} cm^{-2}.[20] We suppose that the trapped charge density in Al_2O_3/GeO_x is attributed to trapping at the O-rich GeO_x layer plus Al_2O_3 oxide trap sites, which is qualitatively and quantitatively different from the significant trapping at Ge-rich GeO_x in HfO_2 stacks. It is very clear in the band diagram that the charge trapping at the VB potential well in the O-rich GeO_x layer should be much less than that in the Ge-rich GeO_x layer in HfO_2 since there are much higher injection barrier height for holes from substrate to the potential well than Ge-rich GeO_x layer.

Correlation of current experimental data strongly suggests that a different chemistry of the GeO_x interface hinging on high-κ dielectric ALD process is a major factor for the significant charge trapping in HfO_2 or Al_2O_3/GeO_x gate stacks. Regardless of high-κ dielectrics, charge trapping at these interfaces occurs at the much higher level than high-κ/Si gate stack and thus, this study implies that the control of the GeO_x interfacial layers would be particularly crucial to realize high-quality working Ge-n-FET since the mobility of electrons in the inversion layer is essentially limited by scattering with these trapping sites.

In summary, interfaces present at the HfO_2 and $Al_2O_3/GeO_x/Ge$ gate stacks were characterized. The investigation of charge trapping during *C-V* sweeps indicated a larger trapped charge density in the HfO_2/GeO_x gate stack than Al_2O_3/GeO_x. SE and MEIS measurements revealed that HfO_2 deposition induced thicker Ge-rich GeO_x interfacial layer having a low bandgap at 1.8 eV. Conversely, Al_2O_3 stacks showed an abrupt and thinner interfacial layer, without formation of Ge-rich GeO_x. The proposed band alignment of gate stacks suggests that the significant charge trapping to band potential wells of Ge-rich GeO_x for HfO_2 accommodating more amount of injected charges, while O-rich GeO_x is responsible for a relatively less charge trapping for Al_2O_3. Therefore, these results strongly suggest that the control of the GeO_x interface layers is crucial to suppress high charge trapping at high-κ/Ge gate stacks.

ACKNOWLEDGMENTS

We gratefully acknowledge the technical advice of J. H. Lee and Y. Yi from Korea Research Institute of Standards and Science (KRISS).

[1] A. Ritenour, A. Khakifirooz, D. A. Antoniadis, R. Z. Leia, W. Tsai, A. Dimoulas, G. Mavrou, and Y. Panayiotatos, Appl. Phys. Lett. **88**, 132107 (2006).
[2] V. V. Afanas'ev, Y. G. Fedorenko, and A. Stesmans, Appl. Phys. Lett. **85**, 032107 (2005).
[3] C. O. Chui, H. S. Kim, D. Chi, P. C. McIntyre, and K. C. Saraswat, IEEE Trans. Electron Devices **53**, 1509 (2006).
[4] M. Caymax, S. Van Elshocht, M. Houssa, A. Delabie, T. Conard, M. Meuris, M. M. Heyns, A. Dimoulas, S. Spiga, M. Fanciulli, J. W. Seo, and L. V. Goncharova, Mater. Sci. Eng., B **135**, 256 (2006).
[5] A. Dimoulas, G. Vellianitis, G. Mavrou, E. K. Evangelou, and A. Sotiropoulos, Appl. Phys. Lett. **86**, 223507 (2005).
[6] B. Kaczer, B. De Jaeger, G. Nicholas, K. Martens, R. Degraeve, M. Houssa, G. Pourtois, F. Leys, M. Meuris, and G. Groeseneken, Microelectron. Eng. **84**, 2067 (2007).
[7] A. Delabie, F. Bellenger, M. Houssa, Th. Conard, S. Van Elshocht, M. Caymax, M. Heyns, and M. Meuris, Appl. Phys. Lett. **91**, 082904 (2007).
[8] K. B. Chung, J. P. Long, H. Seo, and G. Lucovsky, J. Appl. Phys. (to be published).
[9] M. Houssa, L. Pantisano, L.-A. Ragnarsson, R. Degraeve, T. Schram, G. Pourtois, S. De Gendt, G. Groeseneken, and M. M. Heyns, Mater. Sci. Eng. R. **51**, 37 (2006).
[10] G. Lucovsky, H. Seo, S. Ulrich, J. Luning, P. Lysaght, and G. Bersuker, Jpn. J. Appl. Phys., Part 1 **46**, 1899 (2007).
[11] D. E. Aspnes, Proc. SPIE **276**, 188 (1981).
[12] D. E. Aspnes and J. B. Theeten, J. Appl. Phys. **50**, 4928 (1979).
[13] K. I. Seo, P. C. McIntyre, S. Sun, D. I. Lee, P. Pianetta, and K. C. Saraswat, Appl. Phys. Lett. **87**, 042902 (2005).
[14] V. V. Afanas'ev, A. Stesmans, A. Delabie, F. Bellenger, M. Houssa, and M. Meuris, Appl. Phys. Lett. **92**, 022109 (2008).
[15] G. Lucovsky and J. C. Phillips, Microelectron. Reliab. **45**, 770 (2005).
[16] G. S. Armatas and M. G. Kanatzidis, Nature (London) **441**, 04833 (2006).
[17] J. Beynon, M. M. A. G. El-Samanoudy, and S. K. J. Al-Ani, J. Mater. Sci. Lett. **8**, 786 (1989).
[18] Y. Kido and T. Koshikwa, J. Appl. Phys. **67**, 187 (1990).
[19] M. Houssa, G. Pourtois, B. Kaczer, B. De Jaeger, F. Leys, D. Nelis, K. Paredis, A. Vantomme, M. Caymax, M. Meuris, and M. Heyns, Microelectron. Eng. **84**, 2267 (2007).
[20] I. Crupi, R. Degraeve, B. Govoreanu, D. P. Brunco, P. Roussel, and J. Van Houdt, Microelectron. Reliab. **47**, 770 (2007).